Neutron-proton elastic scattering between 200 and 500 MeV. I. Experimental details and measurements of the D_t and P parameters

A. S. Clough and D. R. Gibson*
University of Surrey, Guildford, United Kingdom

D. Axen, R. Dubois, L. Felawka, R. Keeler, G. A. Ludgate, and C. J. Oram
University of British Columbia, Vancouver, Canada

C. Amsler,† D. V. Bugg, and J. A. Edgington
Queen Mary College, London, United Kingdom

L. P. Robertson
University of Victoria, Victoria, Canada

N. M. Stewart
Bedford College, London, United Kingdom

J. Beveridge
TRIUMF, Vancouver, Canada

J. R. Richardson
University of California, Los Angeles, California 90024
(Received 12 March 1979)

Measurements over an extensive angular range of the D_t and P parameters in free neutron-proton elastic scattering at laboratory energies of 220, 325, 425, and 495 MeV are reported. Experimental and analytical details are given.

[NUCLEAR REACTIONS $p(\vec{n}, \vec{p})n$, E= 220, 325, 425, and 495 MeV; measured $D_t(\theta)$, $P(\theta)$.]

I. INTRODUCTION

In their recent phase shift analysis of neutron-proton elastic scattering Arndt, Hackman, and Roper[1] pointed out the paucity of triple scattering parameter data at energies up to 500 MeV. The results presented here for the parameter D_t (a measure of the transfer of polarization from neutron to proton perpendicular to the scattering plane) in free n-p scattering at laboratory energies of 220, 325, 425, and 495 MeV partially rectify that situation. The energies were chosen to correspond to the availability of previous data on elastic nucleon-nucleon scattering. The parameter to be measured, the angular range and the accuracy required were determined by iterative phase shift analysis of existing world data, adding hypothetical data and observing the effect on the phase shift solution. From this procedure it became clear that a measurement of $D_t(\theta)$ to ± 0.03 over a center-of-mass range from 55° to 125° neutron angle θ would provide a strong constraint on the phase shift solution. Measurements to the same accuracy over a wider range, 125° to 180°, while not materially affecting the solution would reduce the errors considerably. Equally useful would be measurements of R_t, A_t (to ± 0.03), and $d\sigma/d\Omega$ (to $\pm 2\%$). Determinations of these other parameters, together with new phase shift solutions, will be presented in subsequent papers.

In this experiment a polarized neutron beam is scattered from an unpolarized hydrogen target. The polarization of the incident beam is either $\pm\langle\sigma_n\rangle$ and is along the direction

$$\vec{n} = \vec{k}_f \times \vec{k}_i ,$$

where $\vec{k}_i, \vec{k}_f$ are the unit momentum vectors of the incident neutron beam and the proton in the final state, respectively. A measure of the scattering rate is

$$(d\sigma/d\Omega)(\theta)[1 \pm P(\theta)\langle\sigma_n\rangle] , \quad (1)$$

where $d\sigma/d\Omega$ is the unpolarized differential cross section and the analyzing power $P \equiv I(n, 0;\ 0, 0)$ in the alternative notation[2] (incident, target; scattered, recoil) for the measured polarizations. When the sign of $\langle\sigma_n\rangle$ is reversed, $P(\theta)$ is deter-

mined with high statistical accuracy from the rate difference. The magnitude of $\langle\sigma_n\rangle$ is determined by two methods which we discuss later.

The magnitude of the polarization of the recoil proton in the $\hat{n}$ direction is given by

$$\langle\sigma_f\rangle = \frac{P'(\theta) \pm D_t(\theta)\langle\sigma_n\rangle}{1 \pm P'(\theta)\langle\sigma_n\rangle}, \qquad (2)$$

where $P' \equiv I(0,0;\ 0,n)$ and $D_t \equiv I(n,0;\ 0,n)$. If the strong interactions are invariant under parity, time reversal, and isospin transformations, $P' \equiv -P$ (although electromagnetic violations of isospin invariance introduce differences between $|P'|$ and $|P|$ of order α). We determine D_t from the change in $\langle\sigma_f\rangle$ under sign reversal of $\langle\sigma_n\rangle$ and the assumption that $P' \equiv -P$.

We also determine P' from the average of $\langle\sigma_f\rangle$ over $\langle\sigma_n\rangle$, but with much lower statistical accuracy than the determination of P and subject to instrumental asymmetry.

II. EXPERIMENTAL METHOD

The experiment was done at TRIUMF, using the 520 MeV sector focused cyclotron. The beamline and apparatus are shown schematically in Figs. 1 and 2.

A. The proton beam

A polarized proton beam of up to 150 nA can be extracted from TRIUMF with an energy between 183 and 520 MeV. Vertically polarized H^- ions are accelerated and, by insertion of a thin carbon foil at a suitable radius, these are stripped to protons which emerge with an energy spread of about 1 MeV. They are transported in vacuum to a focus approximately 3 mm × 3 mm at a deuterium target, and are subsequently swept away by a bending magnet and directed to a beam dump.

The polarization of the beam is continuously monitored by two pairs of counter telescopes MP, selecting p-p elastic scattering coincidences from a 0.05 mm CH_2 foil (see Fig. 1). The small background from p-C interactions has been measured at all energies in a subsidiary experiment.[3] This proton polarimeter also acts as a normalization monitor for the neutron beam intensity.

Random coincidences, typically a few per cent, are monitored continuously, and the appropriate correction is applied. During the setting-up procedure, the primary unpolarized beam is centered on the CH_2 foil and the stability of the polarimeter is checked by displacing the beam by ± 4 mm.

The beam has its polarization direction rotated from the vertical to the horizontal by a superconducting solenoid and is then incident on a 20 cm long by 50 mm diameter cylindrical liquid deuterium target.

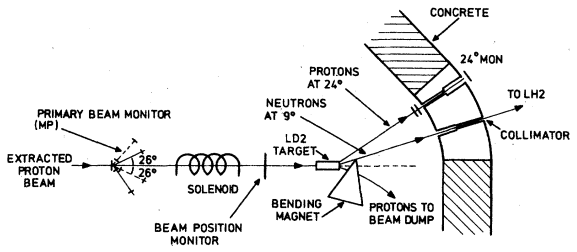

FIG. 1. The proton beamline.

B. The neutron beam

Neutrons are produced by charge exchange scattering, with an energy distribution comprising a high energy quasielastic peak (~ 10 MeV wide) but with a tail down to zero energy. The quasielastic peak is selected by timing with respect to the cyclotron rf. The time of flight cut is 40 to 60 MeV below the peak energy.

The magnitude and orientation of the neutron polarization in the peak as a function of production angle and energy was measured in a separate experiment[4] for incident protons polarized both vertically and horizontally. The optimum polarization transfer to neutrons occurs for horizontally polarized protons at 9° to the incident beam. Hence a neutron beam, which is horizontally polarized, is produced by collimation at this angle sufficient to obtain a beam size full width at half maximum (FWHM) of 7.5 cm diameter at the hydrogen target. An initial collimator consists of two tubular steel sections surrounded by lead and built into a 3.6 m thick concrete and iron shielding wall; both are 1.8 m long, the first being 114 mm diameter and the second 55 mm diameter. The beam then passes through a magnet A with a vertical field which rotates the neutron spin into the beam direction. Within this magnet is a secondary clearing collimator of lead, bored with a hole 450 mm long by 63 mm diameter. The beam then passes through a magnet D with a horizontal field which both rotates the neutron spin into the vertical di-

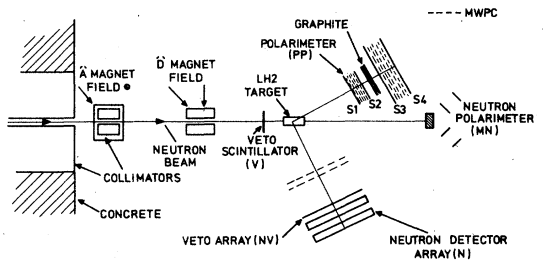

FIG. 2. The neutron beamline and experimental equipment.

rection and sweeps away charged particles in the beam. A subsequent thin scintillator V vetoes any remaining charged particles. The intensity and polariztaion of the neutron beam are monitored continuously by the polarimeter MN, comprising two counter telescopes viewing a thick polythene scatterer, downstream of the hydrogen target. The orientation of the neutron spin was determined[4] at every energy by varying the current in precession magnet A, with D turned off, until the beam was longitudinally polarized. The current in D needed to precess the orientation to the vertical was then set by calculation, using the field values for the precession magnets, which have been measured with an accuracy of ± 1%. Measurements of D_t are insensitive to small errors in this orientation.

C. The hydrogen target

The beam is incident on a cylindrical liquid hydrogen target flask 522 mm long by 110 mm diameter with sides of 0.25 mm Mylar and hemispherical end windows of 0.125 mm Mylar. The flask is wrapped in aluminized Mylar and contained in a vacuum vessel 0.16 m diameter by 0.8 m long with 1.1 mm aluminum alloy sides and two 0.125 mm Mylar end windows upstream and two 0.25 mm Mylar end windows downstream. The complete assembly is surrounded by a gas hood of 0.25 mm plastic for safety reasons. The target can be emptied (to the cold gas) or filled in about ten minutes during a run.

Neutrons and protons resulting from elastic scattering at the target in the horizontal plane are detected by coincidence between a neutron detector and the proton polarimeter positioned at kinematically conjugate angles relative to the hydrogen target, allowing excellent rejection of inelastic scattering.

D. The neutron detector array (N)

This consists of fourteen NE110 scintillation detectors each measuring 1.05 m × 150 mm × 150 mm respectively, with photomultipliers on each square end. Two vertical banks, each of seven horizontal detectors, are placed close together. A face of scintillator 1.05 m × 1.05 m is thus presented to neutrons from the target, with its midpoint at target height. To prevent charged particle detection an array NV of six overlapping scintillators, each 365 mm × 746 mm × 6 mm, is positioned in front of the neutron detectors. The signals from this are put in anticoincidence with signals from any of the neutron detectors.

The vertical position of each interacting neutron is given (to ± 75 mm) by the counter which fires. The horizontal position is measured (to ± 35 mm) by timing the arrival of light at both ends of the scintillator and recording the time difference. For timing purposes, discrimination on pulses from the neutron counter photomultipliers is of the "high-low" type. The timing is taken off the low discriminator level (100 mV) on the anode pulse (passively split to an analog to digital converter for pulse height information). The high threshold is set at a point on the cosmic ray muon spectrum corresponding to 5.3 MeV equivalent electron energy. This procedure was checked by placing the array in a 480 MeV proton beam. The overall detection efficiency of the neutron detector array (which need not be known absolutely) is about 20% for the range of interest, 15–450 MeV.

E. The proton polarimeter (PP)

This measures both the scattering angle of recoil protons and their polarization. It has been described in detail elsewhere[5] and is shown schematically in Fig. 2. Here four 0.5 m × 0.5 m multiwire proportional chambers (MWPC) are located before the 0.5 m × 0.5 m graphite analyzer and six 1 m × 1 m MWPC after it. The graphite is either 60 mm or 30 mm thick, depending on incident proton energy. A coincidence is required between scintillator arrays $S_{1\text{-}4}$ and a neutron detector. The MWPC are then searched electronically and the locations of fired wires stored. The chambers are arranged to give successively, horizontal and vertical information. The times of flight between the accelerator rf and the signal from S_3 (a four scintillator array) are also recorded. These provide the energy selection of the neutron beam mentioned previously.

The solid angles subtended at the target by both the neutron detector array and the proton polarimeter are approximately equal. Both detectors are connected by arms to a point perpendicularly beneath the center of the hydrogen target and can be easily rotated on wheels about this point.

F. Monitors

The beam intensity is monitored in three ways, firstly by the polarimeter MP in the primary proton beam, secondly by the polarimeter MN in the neutron beam, thirdly by a simple telescope viewing the deuterium production target at 24° through a hole in the shield wall. Exhaustive tests of their sensitivity to beam movement and polarization direction show that under stable operating conditions these three monitors agree. The first is statistically the best, and is experi-

mentally the one least subject to the beam movement, so it has been used for all results. The other two monitors are relegated to the status of checking the first. Errors in results for P are dictated by the stability of this monitor; from repeated measurements of P the stability is ± 3%.

G. Electronics and data collection

The fast electronics requires a coincidence between the proton scintillators and a neutron scintillator, in anticoincidence with the veto scintillators before the target and the neutron detector array. Use is made of the Rutherford Laboratory MLS electronics[6] for this purpose. The resultant trigger (i.e., $S_1.S_2.S_3.S_4.\overline{NV}.N.\overline{V}$), referred to as a "proton" event, enables the addresses of wires activated in the MWPC to be read. It also starts CAMAC time-to-digital converters, digitizing separately the four S_3 counters with respect to the RF signal.

Time differences between signals from opposite ends of each neutron counter are also recorded. A PDP-11 computer is programmed to read the CAMAC units, on receipt of the trigger, and store information associated with each event. This information is transferred to magnetic tape in blocks of 40 events and the use of "double buffering" allows events to be recorded at a rate exceeding 30 s^{-1} before the dead time becomes excessive. At the end of a data collection run, scaler information from the various monitors and event counters is read to tape. Data are collected cyclically with incident beams of opposite polarity (achieved by reversing the polarization of the cyclotron ion source), hydrogen target full and empty. Brief runs with an unpolarized beam allow any instrumental asymmetry in the polarimeter MP to be corrected.

III. ANALYSIS AND RESULTS

No on-line analysis or rejection of data is attempted. All events corresponding to a charged particle into the polarimeter PP and a neutral particle into the neutron counter array N are recorded. (All analysis is done off-line using IBM 370 computers at the University of British Columbia, Vancouver and the Rutherford Laboratory, United Kingdom.)

The first step in the analysis is to align the chambers of the polarimeter PP. This is done by analyzing straight track data (taken with the graphite scatterer removed) to determine the small lateral and vertical corrections required to align the chambers relative to each other. Together with measurement of the positions of the polarimeter and neutron array relative to the hydrogen target this fixes the overall alignment of the apparatus. Second, the relationship of the time difference between signals from each end of a neutron detector to the position of neutron interaction is ascertained. This is done by using data taken with a trigger identifying charged particles entering the neutron array and a coincident neutron entering the polarimeter array. We refer to this trigger, $\overline{S}_1.\overline{S}_2.S_3.S_4.NV.N.\overline{V}$, as a neutron event. The proton distributions in the neutron counters map out the widths and positions of each of the six coincident NV counters. These are easily correlated with time differences between signals from opposite ends of each neutron detector.

All the geometrical information from these two procedures, together with information for each event, is analyzed by a program NEUTRON 1. This reconstructs each event to a scattering origin in the liquid hydrogen target, using relativistic kinematics; it assumes the incident beam neutrons arrive parallel to the beam axis and that the event is elastic. For each run it produces histograms of lateral, vertical, and longitudinal positions of event origins. It also histograms distributions of the four S3-rf time-of-flight differences to allow alignment of their peak positions after visual inspection. Acceptance limits on the origin of events in the region of the hydrogen target are decided by visual inspection of the histograms in three dimensions. Inelastic events within this acceptance are $< 0.1\%$ of elastic events. Events are then processed by two routes, the first determining $P(\theta)$ the second determining $D_t(\theta)$.

A. Determination of $P(\theta)$

Preliminary study of histograms allows loose three-dimensional cuts on the origin of the event to be applied by NEUTRON1 and a new data tape generated. A second program bins the data into suitable angular ranges and applies the time-of-flight cuts determined by visual inspection of the NEUTRON1 output. The parameter $P(\theta)$ is then calculated from the difference in numbers of events scattered with neutron beam polarizations of opposite sign, as follows from Eq. (1):

$$P(\theta) = (Z^+ - Z^-)/(\langle\sigma_n^+\rangle Z^- + \langle\sigma_n^-\rangle Z^+)\,, \tag{3}$$

with

$$Z = N_F(\theta)/M_F - N_E(\theta)/M_E\,,$$

where $N^{\pm}(\theta)$ is the number of events in a bin at neutron c.m. angle θ with the incident neutron polarization (of magnitude $\langle\sigma_n^{\pm}\rangle$) up or down; $M^{\pm}$ is the monitor count, corrected for random coincidences, recorded by the sum of the arms of the

polarimeter MP in the primary proton beam; the subscripts F and E indicate hydrogen target full and empty, respectively. This expression yields the correct sign of $P(\theta)$ for neutron events. For proton events the sign has to be reversed.

The neutron beam polarization $\langle\sigma_n\rangle$ is given by

$$\langle\sigma_n\rangle = \frac{\epsilon_P r}{P_{PP}(26^\circ)}.$$

Here ϵ_P is the left-right asymmetry of the polarimeter MP, corrected for randoms and carbon background; P_{PP} (26°) is the P parameter in proton-proton scattering evaluated at the 26° lab angle from previous data[7]; r is the polarization transfer from the proton beam to the neutron beam produced at 9° lab angle. We do not measure this directly, and other data must be used in order to determine $\langle\sigma_n\rangle$ and hence $P(\theta)$, absolutely.

B. The normalization of $\langle\sigma_n\rangle$ and $P(\theta)$

Values of $P(\theta)$ may be normalized to those of Cheng *et al.*[8] and Tinlot *et al.*[9] The former claim a normalization uncertainty of ± 3%. They measured quasielastic p-n scattering. Their results for quasielastic p-p scattering agree well with their results for free p-p scattering. We have checked their normalization for free p-p scattering at 24° lab[7] and agree within their quoted errors of ± 3%. Hence one can have some confidence in their normalization for p-n scattering. Likewise, our normalization for p-p scattering agrees well with the values of Tinlot *et al.*

Alternatively r may be calculated. In the scattering at the deuterium target there is polarization transfer r_t transverse to, and r_t' parallel to the neutron beam direction. Our procedure for finding the orientation of $\langle\sigma_n\rangle$, described earlier for the neutron beam, selects a magnet current in precession magnet A which maximizes the transverse polarization. Thus,

$$r = (r_t^2 + r_t'^2)^{1/2},$$

where r_t, r_t' may be evaluated from free n-p scattering amplitudes, taking into account the final state interactions of the two protons following the method of Cromer[10] as applied in the work of Reay *et al.*[11] They differ by a small amount from the free values $R_t(\theta')$, $R_{t'}(\theta')$ where θ' is the c.m. angle corresponding to the 9° lab production angle.

We combine these two approaches by first performing a phase shift analysis of our P, D_t data (together with measurements of R_t, A_t reported in an accompanying paper[12]), normalizing results with the absolute data of Cheng *et al.*, and Tinlot *et al.* We then evaluate r_t, r_t' from resulting amplitudes calculated at the angle θ' following the method of Cromer. Hence we calculate $\langle\sigma_n\rangle$. We find there is then a small (3%) conflict between normalization of P, D_t, R_t, A_t using the data of Cheng *et al.*, and Tinlot *et al.* and normalization using the derived value of $\langle\sigma_n\rangle$. We accord each equal weight and iterate a phase shift analysis of the data to consistency. Resulting values of r are given in Table I.

C. Results for $P(\theta)$

Values of P thus deduced agree well with values of the polarization P', measured by the polarimeter PP in this experiment (subject to a small instrumental asymmetry) within the statistical precision of the latter measurement (± 6%). They are lower than the values of Cheng *et al.*, and by Tinlot *et al.*, roughly one standard deviation (± 3%).

Statistical errors on $P(\theta)$ are very small, typically ± 0.006. However, the errors are dominated by stability of the intensity monitors. From determinations of P in different runs, from overlapping angular settings of the equipment, and from comparison of neutron and proton events we estimate an error of ± 0.011 in every determination due to monitor instability. This error has been added in quadrature to every determination. Where we have several results within a few degrees, they have been combined, and the weighted mean is given in Table II. Results are shown in Fig. 3, together with the phase shift fits.[13]

D. Determination of $D_t(\theta)$

To obtain a measure of $D_t(\theta)$, more stringent cuts are applied to events. First, within NEUTRON 1, events are selected with a scattering angle greater than 4° in the carbon, to eliminate multiple Coulomb scattering. A tape of remaining events is generated and this is processed by a program NEUTRON 2.

This program applies cuts on the three-dimensional origin of events, corrects individual *S3-RF* times of flight, and writes information about each event to a final tape. This consists primarily of the polar and azimuthal scattering angles (θ, ϕ) of protons emerging from the liquid hydrogen target, the polar and azimuthal scattering

TABLE I. Values of r as a function of neutron energy.

E_n (MeV)	r
220	−0.840
325	−0.853
425	−0.809
495	−0.725

TABLE II. Values of $P(\theta)$ for different incident neutron lab energies (E_n).

E_n (MeV)	θ (deg.)	$P(\theta)$	E_n (MeV)	θ (deg.)	$P(\theta)$
220	49.6	0.170 ± 0.182	325	44.99	0.283 ± 0.026
	56.3	0.300 ± 0.065		50.08	0.266 ± 0.015
	63.2	0.378 ± 0.031		55.21	0.228 ± 0.014
	70.2	0.267 ± 0.025		60.31	0.143 ± 0.014
	76.9	0.127 ± 0.025		66.39	0.077 ± 0.013
	83.9	0.057 ± 0.026		71.50	−0.022 ± 0.021
	96.9	−0.080 ± 0.017		78.23	−0.083 ± 0.011
	104.0	−0.096 ± 0.017		83.00	−0.124 ± 0.010
	111.1	−0.126 ± 0.017		87.90	−0.150 ± 0.008
	118.3	−0.129 ± 0.017		94.70	−0.204 ± 0.008
	125.5	−0.127 ± 0.017		100.53	−0.225 ± 0.007
	132.7	−0.133 ± 0.015		106.05	−0.226 ± 0.008
	140.0	−0.130 ± 0.018		112.21	−0.207 ± 0.009
	147.3	−0.127 ± 0.017		118.39	−0.211 ± 0.007
	154.7	−0.121 ± 0.017		124.05	−0.168 ± 0.007
	162.1	−0.122 ± 0.031		129.78	−0.167 ± 0.008
				136.48	−0.128 ± 0.007
				142.30	−0.120 ± 0.007
				147.84	−0.104 ± 0.008
				153.80	−0.095 ± 0.012
				159.40	−0.086 ± 0.040
425	34.60	0.255 ± 0.054	495	34.10	0.203 ± 0.074
	41.00	0.325 ± 0.026		40.50	0.402 ± 0.034
	47.60	0.288 ± 0.016		46.90	0.330 ± 0.021
	54.20	0.238 ± 0.016		53.50	0.219 ± 0.023
	60.53	0.137 ± 0.012		59.41	0.157 ± 0.013
	67.13	0.063 ± 0.011		66.05	0.082 ± 0.014
	73.47	−0.010 ± 0.010		72.70	−0.007 ± 0.014
	80.83	−0.090 ± 0.009		79.40	−0.072 ± 0.012
	87.45	−0.155 ± 0.008		86.30	−0.149 ± 0.012
	94.54	−0.213 ± 0.008		93.40	−0.216 ± 0.013
	101.67	−0.236 ± 0.008		100.65	−0.265 ± 0.015
	108.53	−0.247 ± 0.008		108.01	−0.264 ± 0.014
	116.09	−0.233 ± 0.009		115.38	−0.284 ± 0.014
	123.44	−0.200 ± 0.010		122.83	−0.268 ± 0.015
	130.80	−0.161 ± 0.012		131.55	−0.190 ± 0.016
	138.30	−0.125 ± 0.012		137.70	−0.147 ± 0.017
	145.90	−0.111 ± 0.012		145.40	−0.129 ± 0.012
	153.50	−0.080 ± 0.016		153.10	−0.090 ± 0.016
	161.20	−0.076 ± 0.017		160.90	−0.076 ± 0.016
	168.90	−0.070 ± 0.026			

angles (Θ, Φ) of these same protons in the graphite sheet, and the time of flight of the incident neutron. Information is also recorded about the azimuthal acceptance of the polarimeter for scatters from the graphite, as this will differ for each event. It is in the form of up to eight azimuthal angles $\{\Phi_1-\Phi_8\}$, at which a circle about the track of the incident proton at angle Θ intersects the square outline of S_4. An example, for a perpendicularly incident track, is shown in Fig. 4. In this example $\Phi_4, \Phi_5, \Phi_6, \Phi_7$, do not exist. This final tape is then processed separately by programs which independently produce evaluations of $D_t(\theta)$ by two different methods.

Method 1. The polarization of the outgoing protons $\langle\sigma_f^{\pm}(\theta)\rangle$ for incident neutron beam polarization $\pm\langle\sigma_n^{\pm}\rangle$ up or down is related to $P(\theta)$, $D_t(\theta)$ by

$$\langle\sigma_f^{\pm}(\theta)\rangle = \frac{-P(\theta) \pm D_t(\theta)\langle\sigma_n^{\pm}\rangle}{1 \mp P(\theta)\langle\sigma_n^{\pm}\rangle}. \tag{4}$$

Measurement of $\langle\sigma_f(\theta)\rangle$ is subject to any instrumental asymmetry in the polarimeter, present for both spin-up and -down runs. This may be eliminated to second order and $D_t(\theta)$ evaluated by taking the difference

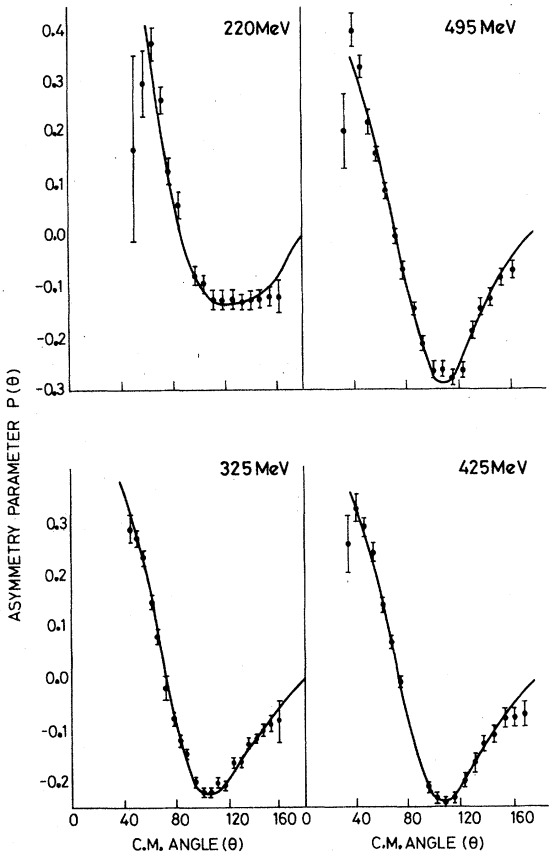

FIG. 3. Results for $P(\theta)$, fitted by phase shift analysis (Ref. 13).

$$\langle\sigma_f^+(\theta)\rangle - \langle\sigma_f^-(\theta)\rangle$$

$$= -P(\theta)\left(\frac{1}{1-P(\theta)\langle\sigma_n^+\rangle} - \frac{1}{1+P(\theta)\langle\sigma_n^-\rangle}\right)$$

$$+D_t(\theta)\left(\frac{\langle\sigma_n^+\rangle}{1-P(\theta)\langle\sigma_n^+\rangle} + \frac{\langle\sigma_n^-\rangle}{1+P(\theta)\langle\sigma_n^-\rangle}\right). \quad (5)$$

The first term on the right-hand side is numerically small, and is evaluated from values of $P(\theta)$ interpolated from Table I.

If protons were incident perpendicularly at the center of the carbon, analysis of the distribution of scattered particles to determine $\langle\sigma_f\rangle$ would be straightforward. The number scattered at angle $\{\Theta, \Phi\}$ would be

$$N(\Theta,\Phi) \propto [1+\langle\sigma_f\rangle A_c(\Theta)\cos\Phi]\eta(\theta,\Phi),$$

where $A_c(\Theta)$ is the analyzing power of carbon and $\eta(\Theta,\Phi)$ is the detection efficiency of the polarimeter at this angle (either approximately unity or, in the case that the proton misses S_4, zero). Hence one could obtain a measure of $\langle\sigma_f\rangle$, correct to first order in $\eta(\Theta,\Phi)$ by forming the ratio

$$\frac{1}{A_c(\Theta)\cos\Phi}\,\frac{N(\Theta,\Phi)-N(\Theta,\pi-\Phi)}{N(\Theta,\Phi)+N(\Theta,\pi-\Phi)},$$

with a statistical error

$$\frac{1}{[N(\Theta,\Phi)+N(\Theta,\pi-\Phi)]^{1/2}A_c(\Theta)\cos\Phi}.$$

The statistically best estimate of $\langle\sigma_f\rangle$ is evaluated by forming the weighted mean over all pairs of angles $\{\Phi, \pi-\Phi\}$:

$$\langle\sigma_f\rangle = \frac{\sum_{\Theta,\Phi} A_c(\Theta)\cos\Phi[N(\Theta,\Phi)-N(\Theta,\pi-\Phi)]}{\sum_{\Theta,\Phi} A_c{}^2\cos^2\Phi[N(\Theta,\Phi)+N(\Theta,\pi-\Phi)]}.$$

This procedure can be simply extended to the situation where protons are incident at angles other than 90° and at positions all over the carbon face by accepting only those events at an angle $\{\Theta,\Phi\}$, relative to the incident proton direction, for which events at supplementary Φ angle $\{\Theta, \pi-\Phi\}$ are within the geometrical acceptance. This information is present for each event in the angles Φ_{1-8}.

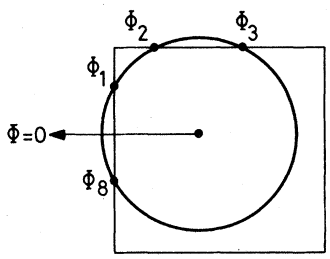

FIG. 4. Example of Φ_i definition.

TABLE III. Values of coefficients in the detection efficiency expansion as a function of neutron energy.

E_n (MeV)	α_1	α_2	α_3	β_1	β_2
220	0.000 ± 0.013	−0.027 ± 0.013	0.019 ± 0.013	−0.010 ± 0.013	0.008 ± 0.013
325	0.008 ± 0.008	0.007 ± 0.008	0.000 ± 0.008	−0.006 ± 0.008	−0.012 ± 0.008
425	0.009 ± 0.006	0.003 ± 0.006	0.017 ± 0.006	0.003 ± 0.006	0.001 ± 0.006
495	0.009 ± 0.008	0.029 ± 0.008	0.026 ± 0.008	−0.002 ± 0.008	0.006 ± 0.008

The quantity $\langle \sigma_f^{\pm}(\theta) \rangle$ is evaluated thus for spin-up and -down runs separately and $D_t(\theta)$ is evaluated from their difference after application of a target empty subtraction.

Method 2. A second method, of quite general applicability but greater computational complexity which allows the use of all events, has also been developed. The method is described in detail elsewhere,[14] but will be outlined here.

The technique used is that of point estimation of parameters. A set of azimuthal probability distributions is written down, one for each event, of the form

$$P_i(\Phi) = \frac{1}{C_i} [1 + \langle \sigma_f \rangle A_c(\Theta) \cos\Phi] \eta(\Theta.\Phi) .$$

Since each event samples a different azimuthal acceptance, determined by the values of the intercept azimuths $\Phi_1 - \Phi_8$, correct normalization requires that each event be linked with a different normalization constant, say C_i for the ith event. Each C_i is a function of the quantities of interest $\langle \sigma_f \rangle$ and $\eta(\Theta, \Phi)$, as well as of the known quantities

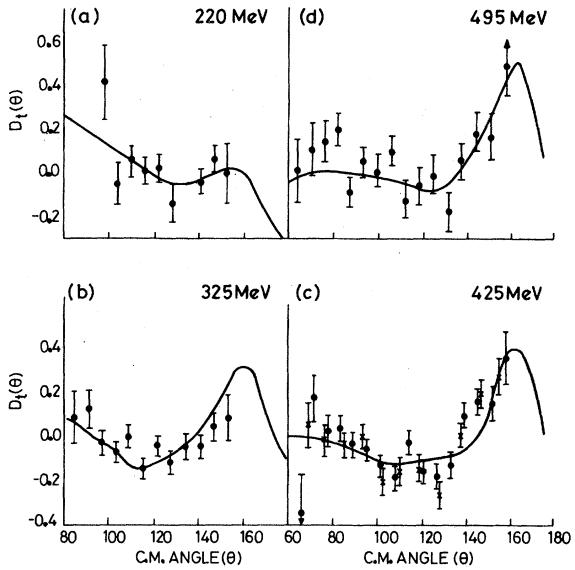

FIG. 5. Results for $D_t(\theta)$ from Method 2 (dots) and Method 1 (crosses), fitted by phase shift analysis (Ref. 13).

TABLE IV. Values of $D_t(\theta)$ for different neutron energies.

E_n (MeV)	θ (deg.)	$D_t(\theta)$	E_n (MeV)	θ (deg.)	$D_t(\theta)$
220	98.3	0.402 ± 0.160	325	84.15	0.074 ± 0.117
	104.1	−0.052 ± 0.089		90.30	0.110 ± 0.086
	110.0	0.054 ± 0.068		96.80	−0.042 ± 0.054
	116.2	0.009 ± 0.059		102.40	−0.080 ± 0.047
	122.1	0.022 ± 0.060		108.70	−0.010 ± 0.049
	128.0	−0.136 ± 0.084		115.00	−0.153 ± 0.045
	135.3	−0.029 ± 0.080		121.20	−0.053 ± 0.043
	141.1	−0.041 ± 0.056		127.10	−0.129 ± 0.051
	147.0	0.064 ± 0.063		134.00	−0.055 ± 0.057
	152.5	0.002 ± 0.133		140.20	−0.052 ± 0.050
				146.20	0.033 ± 0.063
				152.87	0.073 ± 0.102
425	65.7	−0.364 ± 0.184	495	59.9	−0.195 ± 0.281
	71.3	0.157 ± 0.107		64.6	0.015 ± 0.144
	77.4	0.010 ± 0.073		70.7	0.107 ± 0.119
	83.1	0.021 ± 0.057		76.6	0.141 ± 0.092
	89.0	−0.050 ± 0.054		82.3	0.197 ± 0.072
	95.2	−0.076 ± 0.049		88.2	−0.086 ± 0.067
	101.2	−0.148 ± 0.049		94.3	0.049 ± 0.068
	107.9	−0.208 ± 0.050		100.3	0.010 ± 0.074
	114.0	−0.041 ± 0.053		106.9	0.098 ± 0.067
	120.1	−0.174 ± 0.052		113.2	−0.123 ± 0.082
	126.4	−0.193 ± 0.054		119.4	−0.064 ± 0.083
	133.2	−0.147 ± 0.056		125.8	−0.009 ± 0.088
	139.3	0.081 ± 0.054		132.5	−0.175 ± 0.086
	145.8	0.141 ± 0.060		138.6	0.054 ± 0.077
	152.2	0.135 ± 0.077		145.3	0.189 ± 0.089
	158.1	0.341 ± 0.121		151.9	0.167 ± 0.102
				158.3	0.485 ± 0.133

$\Phi_1 - \Phi_8$. In practice we take $\eta(\Theta, \Phi)$ to be a trigonometric series in Φ with unknown coefficients, each term representing a simple geometrical symmetry of the detector array:

$$\eta = \alpha_0 + \alpha_1 \cos\Phi + \alpha_2 \cos 2\Phi + \alpha_3 \cos 4\Phi + \beta_1 \sin\Phi + \beta_2 \sin 2\Phi .$$

Each C_i is therefore calculable as a function of $\langle \sigma_f \rangle$ and these coefficients. We are then able to write down a set of expectation values for each probability distribution, for example $\langle A_c(\Theta) \cos\Phi \rangle_i$; each such expectation value is of the form $N_i(\Theta, \Phi)/C_i$ where the numerator $N_i(\Theta, \Phi)$ is, like C_i, calculable by integration, given values of the parameters $\langle \sigma_f \rangle$ and the efficiency coefficients. Were the C_i constant from one event to another, each expectation value could be replaced by an appropriate summation over the experimental data, and the equations solved exactly to yield unbiased estimators of the parameters. In fact this is not possible since the expectation values are clearly nonlinear functions of the parameters, owing to the latter's presence in the denominator C_i as well as the numerator $N_i(\Theta, \Phi)$. Instead we solve the equation by iteration, projecting out the larger terms in the various equations to obtain a first approximation to the parameters, and repeating the calculation using these values as input.

Convergence is rapid, and all events contribute to the final results. Not only $\langle \sigma_f \rangle$, but also the various efficiency coefficients are found explicitly. These coefficients are listed in Table III, together with the geometrical symmetry each represents. It is gratifying that these coefficients are, with few exceptions, consistent with zero. Then D_t is evaluated as in Method 1 using Eq. (5). Figure 5(c) illustrates the excellent agreement between the values of D_t obtained by both methods. The second gives the smaller statistical errors, as it utilizes roughly 20% more of the events, and Table IV shows the values of D_t thus obtained. These are plotted in Fig. 5, together with predictions from out final phase shift analysis.[11] (Note that this analysis includes not only these D_t data, but also the values of R_t and A_t presented in the following paper.[13])

E. Results for $P'(\theta)$

Method 1 has been used to determine the polarization P' of the recoil proton as a check on the normalization of $P(\theta)$. Measurements of $\langle \sigma_f(\theta) \rangle$ are averaged over the polarization of the incident neutron beam in such a way as to simulate an unpolarized incident beam. Results are shown graphically in Fig. 6. However, we recommend

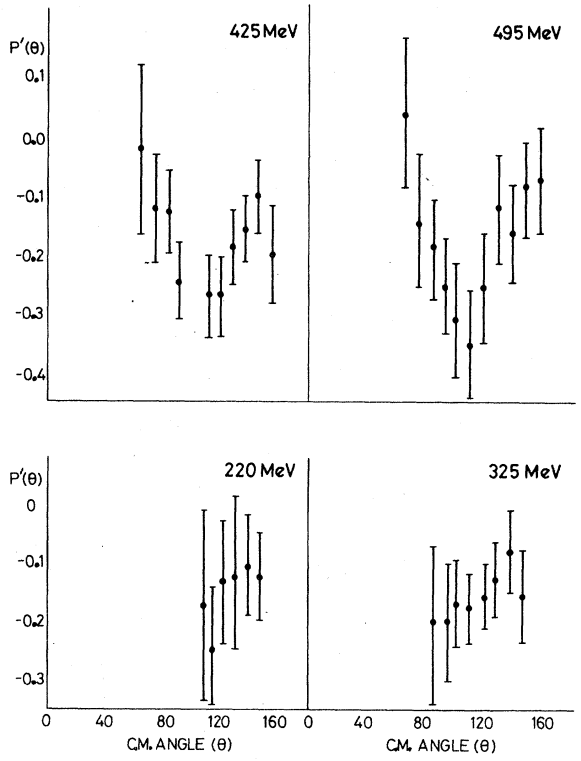

FIG. 6. Results for $P'(\theta)$.

that they should not be used in phase shift analyses since they are subject to instrumental asymmetry in the polarimeter, and values of $P(\theta)$ are statistically superior.

IV. SUMMARY

Accurate values of the P and D_t parameters in free neutron-proton scattering are reported in Tables II and IV for an extensive angular range at lab energies of 220, 325, 425, and 495 MeV. At each energy they share a common normalization uncertainty of $\pm 3\%$. Values of R_t and A_t (Ref. 12) and a phase shift analysis[13] will be reported in subsequent papers.

ACKNOWLEDGMENTS

We are grateful to Professor J. Sample and the staff of TRIUMF for their assistance and efforts in this experiment. We particularly thank Mr. G. Waters for his assistance with the chambers and electronics and Mr. A. Bishop for successfully commissioning and operating the liquid hydrogen target. D.R.G. thanks the Northern Ireland Ministry of Education for financial support. R.K. and R.D. thank the National Research Council of Canada for financial support.

*Now at British Steel Corporation, Sheffield, England.
†Now at University of New Mexico, Albuquerque, New Mexico.

[1]R. A. Arndt, R. H. Hackman, and L. D. Roper, Phys. Rev. C 15, 1002 (1977).
[2]F. Halzen and G. H. Thomas, Phys. Rev. D 10, 344 (1974).
[3]D. V. Bugg *et al.*, J. Phys. G 4, 1025 (1978).
[4]C. Amsler *et al.*, Nucl. Inst. 144, 401 (1977).
[5]G. Waters *et al.*, Nucl. Inst. 153, 401 (1978).
[6]R. S. Milborrow, Rutherford Laboratory Report No. RHEL/M141 (unpublished).
[7]C. Amsler *et al.*, J. Phys. G 4, 1947 (1978).
[8]D. Cheng *et al.*, Phys. Rev. 163, 1470 (1967).
[9]J. H. Tinlot and R. E. Warner, Phys. Rev. 124, 890 (1961).
[10]A. H. Cromer, Phys. Rev. 129, 1680 (1963).
[11]N. W. Reay *et al.*, Phys. Rev. 150, 801 (1966).
[12]D. Axen *et al.*, Phys. Rev. C 21, 998 (1980), this issue.
[13]D. V. Bugg *et al.*, Phys. Rev. C 21, 1004 (1980), this issue.
[14]J. A. Edgington, Nucl. Inst. 164, 175 (1979).